

Cryogenic Ion Spectroscopy of the Green Fluorescent Protein Chromophore in Vacuo

Wyatt Zagorec-Marks, Madison M. Foreman, Jan R. R. Verlet, and J. Mathias Weber

J. Phys. Chem. Lett., **Just Accepted Manuscript** • DOI: 10.1021/acs.jpcllett.9b02916 • Publication Date (Web): 04 Nov 2019

Downloaded from pubs.acs.org on November 13, 2019

Just Accepted

“Just Accepted” manuscripts have been peer-reviewed and accepted for publication. They are posted online prior to technical editing, formatting for publication and author proofing. The American Chemical Society provides “Just Accepted” as a service to the research community to expedite the dissemination of scientific material as soon as possible after acceptance. “Just Accepted” manuscripts appear in full in PDF format accompanied by an HTML abstract. “Just Accepted” manuscripts have been fully peer reviewed, but should not be considered the official version of record. They are citable by the Digital Object Identifier (DOI®). “Just Accepted” is an optional service offered to authors. Therefore, the “Just Accepted” Web site may not include all articles that will be published in the journal. After a manuscript is technically edited and formatted, it will be removed from the “Just Accepted” Web site and published as an ASAP article. Note that technical editing may introduce minor changes to the manuscript text and/or graphics which could affect content, and all legal disclaimers and ethical guidelines that apply to the journal pertain. ACS cannot be held responsible for errors or consequences arising from the use of information contained in these “Just Accepted” manuscripts.

1
2
3
4
5
6
7
8
9
10
11
12
13
14
15
16
17
18
19
20
21
22
23
24
25
26
27
28
29
30
31
32
33
34
35
36
37
38
39
40
41
42
43
44
45
46
47
48
49
50
51
52
53
54
55
56
57
58
59
60

Cryogenic Ion Spectroscopy of the Green Fluorescent Protein Chromophore in Vacuo

Wyatt Zagorec-Marks,¹ Madison M. Foreman,¹ Jan R. R. Verlet,² J. Mathias Weber^{1,}*

¹JILA and Department of Chemistry, University of Colorado, Boulder, CO 80309-0440, USA.

²Department of Chemistry, Durham University, Durham, DH1 3LE, UK.

AUTHOR INFORMATION

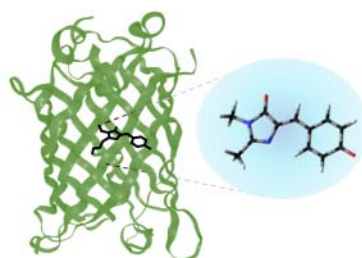
Corresponding Author

*E-mail: weberjm@jila.colorado.edu. Tel.: +1-303-492-7841

1
2
3 **ABSTRACT.** We present the spectrum of the $S_1 \leftarrow S_0$ transition of an anionic model for the
4 chromophore of the green fluorescent protein *in vacuo* at cryogenic temperatures, showing
5 previously unresolved vibrational features, and resolving the band origin at 20930 cm^{-1} (477.8 nm)
6 with unprecedented accuracy. The vibrational spectrum establishes that the molecule is in the *Z*
7 isomer at low temperature. At increased temperature, the $S_1 \leftarrow S_0$ band shifts to the red, which we
8 tentatively attribute to emergent population of the *E* isomer.
9
10
11
12
13
14
15
16
17
18
19
20

21 TOC GRAPHICS

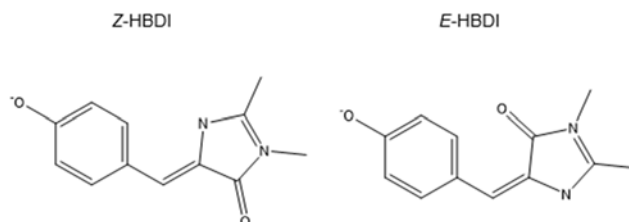
22
23
24
25
26
27
28
29
30
31
32
33
34
35
36
37
38
39
40
41
42
43
44
45
46
47
48
49
50
51
52
53
54
55
56
57
58
59
60



1
2
3
4
5
6
7
8
9
10
11
12
13
14
15
16
17
18
19
20
21
22
23
24
25
26
27
28
29
30
31
32
33
34
35
36
37
38
39
40
41
42
43
44
45
46
47
48
49
50
51
52
53
54
55
56
57
58
59
60

Fluorescent proteins have become a work-horse for fluorescence labeling in biology,¹⁻⁵ with the Green Fluorescent Protein (GFP) and its variants being the most widely used for monitoring *in vivo* processes. The fluorescence originates from a small chromophore in the protein consisting of a phenol ring linked by a methine bridge at the *para*-position to an imidazole ring. The neutral and deprotonated (anionic) chromophores have absorption maxima around 395 nm and 480 nm, respectively,⁶⁻⁷ but only the anion fluoresces as the neutral form undergoes excited state proton transfer.⁷ A widely used model for the GFP chromophore is deprotonated *p*-hydroxybenzylidene-2,3-dimethylimidazolinone (HBDI⁻, see Scheme 1), where the anchoring points to the protein are replaced by two methyl groups on the imidazole moiety. In contrast to the protein, HBDI⁻^{8-9,10} undergoes twisting around the bonds of the methine bridge during relaxation on the S₁ excited state in low viscosity solvents⁸⁻⁹ and *in vacuo*¹⁰ and fluorescence is lost. The same twisting motions also give rise to two isomeric forms, *Z*-HBDI⁻ and *E*-HBDI⁻ (see Scheme 1). In fact, the Dronpa protein, which has the same chromophore as GFP, can be photoswitched between the fluorescent *Z* isomer and the non-fluorescent *E* isomer.¹¹⁻¹²

The S₁ ← S₀ absorption profile contains details about the initial S₁ excited state photophysics of HBDI⁻ and its interactions with the protein or solvent environment. Consequently, there have been many studies of HBDI⁻ *in vacuo* in an attempt to understand the intrinsic photophysics. The first spectrum of isolated HBDI⁻ showed striking similarities with the protein suggesting that the sum of the interactions with the protein environment results in initial photophysics closer to vacuum than to aqueous solution. However, the photodissociation spectra presented to date have all been obtained at elevated temperature, obscuring many details of the intrinsic S₁ ← S₀ absorption profile.

Scheme 1. *Z* and *E* isomers of HBDF⁻.

The intrinsic photophysics of HBDF⁻ has been mostly investigated through photodissociation and photoelectron spectroscopies,^{8-10, 13-36} as the relaxation from the S₁ excited state predominantly results in dissociation or electron loss. Photodissociation of bare HBDF⁻ occurs after relaxation to the electronic ground state, which produces a vibrationally hot ion that decays primarily through the loss of a CH₃ group. For dissociation to be observable on a microsecond time scale, two photons in the visible spectral region need to be absorbed,¹³ as one-photon dissociation occurs on a millisecond time scale.¹⁵ Moreover, the threshold for electron detachment is only slightly higher (2.73 eV,³⁷ or 22017 cm⁻¹) than the peak of the photodissociation spectrum at room temperature measured at around 480 nm (2.58 eV, or 20833 cm⁻¹). As a result, electron detachment and dissociation are competing relaxation pathways upon photoexcitation, and detachment can proceed directly or through vibrational autodetachment, the latter of which is thought to dominate.^{10, 18-21, 24, 26-28, 31} At 300 K, HBDF⁻ stores ca. 390 meV in vibrational energy, which contributes to any statistical process. Hence, the interpretation of photodestruction experiments conducted to date has been complicated by a mixture of competing processes that have led to a debate in the literature since the first photodestruction spectrum of HBDF⁻ was published in 2001.¹³ Adding to this debate, a recent study by Bieske and coworkers³⁴ showed that under common preparation conditions, a significant fraction of the HBDF⁻ ions is in the *E* isomeric

1
2
3 form, while the interpretation of experimental data and computational efforts have largely focused
4 on the *Z* isomer. To overcome these ambiguities, here we present cryogenic spectra of bare and
5 messenger-tagged HBDI^- in the infrared and visible spectral regions, supported by density
6 functional theory calculations. Our data shows partially resolved vibrational structure of the $S_1 \leftarrow$
7 S_0 transition of HBDI^- and yields accurate values for the band origin. We demonstrate that HBDI^-
8 prepared at low temperature in a cryogenic ion trap exists predominantly as the *Z* isomer. With
9 increasing temperature, the *E* isomer population increases.
10
11
12
13
14
15
16
17
18
19

20 Figure 1 shows the photodissociation action spectrum of the complex $[\text{HBDI}^- \cdot \text{N}_2]$,
21 monitoring the formation of bare HBDI^- by the loss of the weakly-bound N_2 messenger. Messenger
22 loss can be expected to occur with near unit probability upon absorption of a photon down to the
23 far infrared, due to the low binding energy of N_2 (calculated at 630 cm^{-1} on the imidazole moiety,
24 720 cm^{-1} on the phenolate group). Consequently, the presence of N_2 guarantees that the target
25 complexes are cold. The ion temperature can be conservatively estimated to be $< 75 \text{ K}$ by
26 describing cluster formation in the trap as an evaporative ensemble.³⁸ The spectrum of $[\text{HBDI}^-$
27 $\cdot \text{N}_2]$ shows a sharp onset of the photodissociation action signal at $(20530 \pm 25) \text{ cm}^{-1}$, followed by
28 a peak at $(20780 \pm 10) \text{ cm}^{-1}$, and a second peak at $(20835 \pm 10) \text{ cm}^{-1}$. Partially resolved vibrational
29 structure is observed in the spectrum with a spacing of ca. 70 cm^{-1} . An additional feature appears
30 with an onset at 21830 cm^{-1} and a peak at 22130 cm^{-1} .
31
32
33
34
35
36
37
38
39
40
41
42
43
44
45
46
47
48
49
50
51
52
53
54
55
56
57
58
59
60

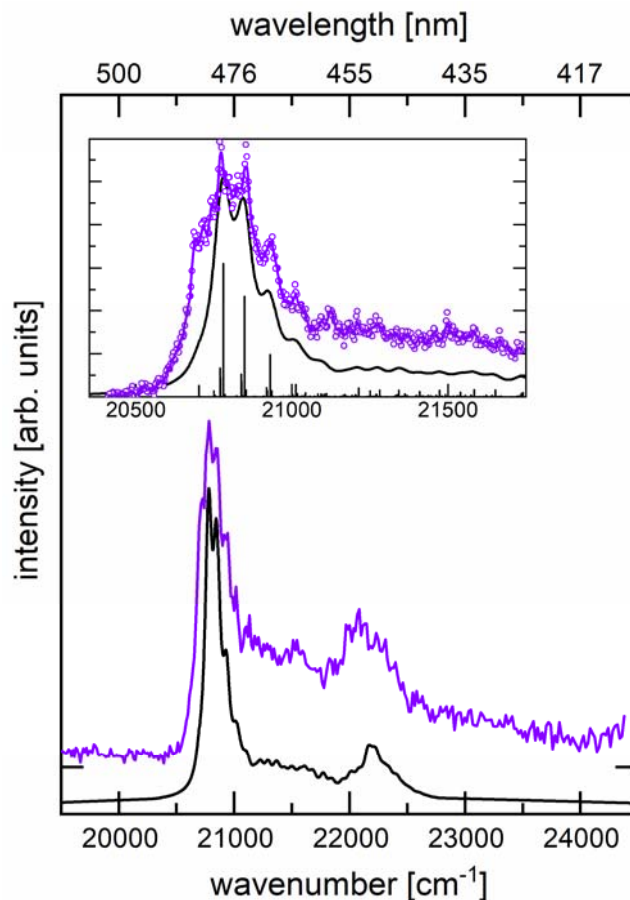


Figure 1. Photodissociation spectrum of [HBDI·N₂]. The open circles are raw data points, the purple full line is a 5-point adjacent average to guide the eye. The black full lines are Franck-Condon-Herzberg-Teller simulations of the vibrational substructure in the S₁ ← S₀ electronic band, with the vibrational states indicated as vertical sticks. The insert focuses on the band origin region, and the data in this trace were taken with a step size of 2.6 cm⁻¹, while the step size in the overview spectrum was 13 cm⁻¹ in the origin region. The simulation has been shifted by ca. -4000 cm⁻¹ for the best match to the experimental spectrum (see Methods section).

To address which isomer is probed, the infrared spectrum of [HBDI·N₂] is shown in Figure 2, together with computed spectra of the *Z* and *E* isomers (scaled harmonic approximation). Although the predicted spectra of the two isomers are very similar, the spacings between the three most intense features in the 1400 – 1700 cm⁻¹ region are distinctly different and match most closely with the *Z* isomer.³⁹ The narrow width of the main features indicates that only one isomer is

1
2
3 significantly populated. The assignment is also consistent with calculations that place the *Z* isomer
4 lower in energy by 100 meV, and with ion mobility experiments that showed only *Z* isomers for
5
6
7
8
9
10
11
12
13
14
15
16
17
18
19
20
21
22
23
24
25
26
27
28
29
30
31
32
33
34
35
36
37
38
39
40
41
42
43
44
45
46
47
48
49
50
51
52
53
54
55
56
57
58
59
60

complexed HBDI⁻ with solvent molecules.³⁴

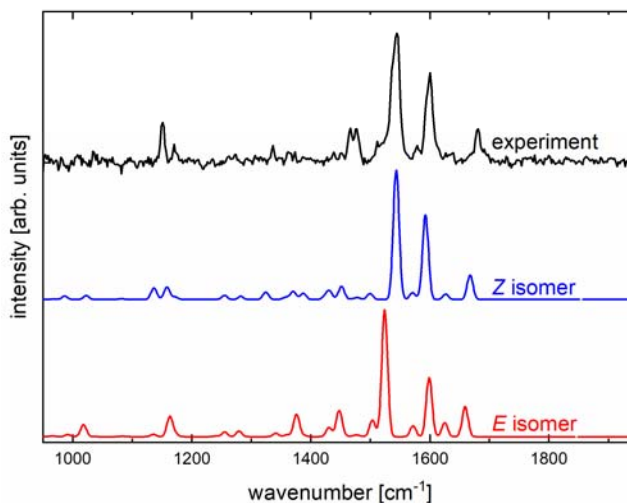


Figure 2. Experimental infrared action spectrum of [HBDI⁻·N₂] (top trace) compared to simulated spectra of the *Z* isomer (center trace) and *E* isomer (bottom trace) of HBDI⁻. The scaling factor for the simulated spectra is 0.98. A detailed assignment of the vibrational features is listed in Table S1 (see Supporting Information).

Figure 1 includes a Franck-Condon-Herzberg-Teller simulation of the $S_1 \leftarrow S_0$ band of the *Z* isomer (shifted to fit the experimental spectrum). The simulation qualitatively recovers the vibrational substructure of the experimental spectrum. The observed quantitative differences are not surprising given the level of theory, but also highlight the opportunity for high-level calculations to recover the S_1 potential energy surface in the Franck-Condon region. The qualitative agreement nevertheless enables us to assign general features. The low-frequency mode (ca. 70 cm⁻¹) corresponds to a methine bridge bending/ring scissoring mode (ω_B , calculated at ca.

1
2
3 80 cm^{-1} on the S_1 surface). We assign the peak at $(20780 \pm 10) \text{ cm}^{-1}$ as the electronic band origin,
4
5 i.e., as the $S_1(v=0) \leftarrow S_0(v=0)$ transition of $[\text{HBDF} \cdot \text{N}_2]$, based on the hot band structure on its
6
7 low-energy side. The broad feature beginning at ca. 21830 cm^{-1} and peaking at $(22130 \pm 40) \text{ cm}^{-1}$
8
9 can be traced to combination bands of ω_B building on an imidazole ring breathing/in-plane CH
10
11 bending mode on the S_1 surface (ω_I , calculated at ca. 1350 cm^{-1}), in accord with previous
12
13 assignments.^{22, 40-41} Congestion in the spectrum is largely caused by the Franck-Condon active ω_B
14
15 mode, which is also responsible for the two hot band shoulders below the band origin and the high-
16
17 energy shoulder on the feature belonging to ω_I . Both ω_B and ω_I have been identified as strongly
18
19 Franck-Condon active modes in earlier computational work, and our calculated spectral profile
20
21 qualitatively agrees with results from other calculations at much higher levels of theory (see
22
23 Supporting Information).^{22, 40-41}
24
25
26
27
28
29

30
31 Note that the width of the experimental vibrational signatures is not limited by the
32
33 experiment (see Methods Section), which is on the order of ca. $5\text{-}10 \text{ cm}^{-1}$.⁴² Our simulation
34
35 suggests that the measured linewidth has a full width at half maximum of about 80 cm^{-1} . This
36
37 broadening is in part due to congestion from other low-frequency modes and due to the intrinsic
38
39 dynamics on the S_1 state leading to lifetime broadening.
40
41

42
43 The spectrum in Figure 1 is that of $[\text{HBDF} \cdot \text{N}_2]$, but the species of interest is bare HBDF .
44
45 Previous experiments using N_2 as a messenger tag⁴³ suggest that the presence of the N_2 tag leads
46
47 to a small overall spectral shift at the same ion trap temperature. The photodissociation spectrum
48
49 of bare HBDF at various trap temperatures is shown in Figure 3 and compared to the spectrum of
50
51 $[\text{HBDF} \cdot \text{N}_2]$. These spectra were acquired by monitoring the loss of CH_3 which is assumed to be a
52
53 two-photon process, as the observation time in our experiment is ca. $20 \mu\text{s}$.
54
55
56
57
58
59
60

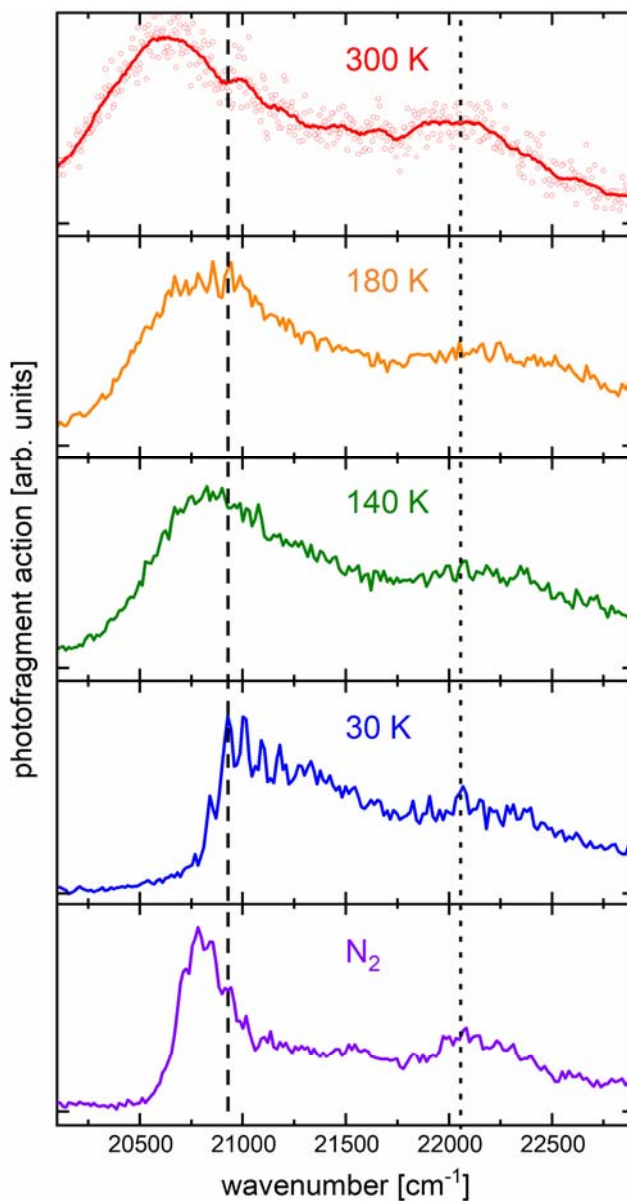


Figure 3. Photodissociation spectra of HBDI⁻ at different trap temperatures. For the spectrum at 300 K, the open circles are raw data points and the full line is a 20-point adjacent average to guide the eye. For the other spectra, the solid line represents the raw data. The vertical dashed and dotted lines shows the peak positions for bare HBDI⁻ (30 K) of the ($\nu = 0$) \leftarrow ($\nu = 0$) band at $(20930 \pm 10) \text{ cm}^{-1}$, and of the high energy feature around 22100 cm^{-1} , respectively.

1
2
3 The spectrum of bare HBDF⁻ at 30 K has an onset at $(20250 \pm 50) \text{ cm}^{-1}$, which is at much
4 lower wavenumbers than that of [HBDF⁻·N₂], and the peak of the spectrum is at (20930 ± 10)
5 cm^{-1} , with partially resolved peaks at lower energies. At the high-energy side of this peak,
6 vibrational features are observed, with a spacing commensurate with that found in the spectrum of
7 [HBDF⁻·N₂]. We assign the peak at 20930 cm^{-1} (ca. 477.8 nm) to the $S_1(v=0) \leftarrow S_0(v=0)$ transition
8 of bare HBDF⁻.
9
10
11
12
13
14
15
16
17

18 The presence of the first N₂ tag shifts the spectrum by $(150 \pm 27) \text{ cm}^{-1}$ to the red; a second
19 N₂ tag leads to an additional $(80 \pm 27) \text{ cm}^{-1}$ red-shift (measured from the highest point in the band
20 envelope, see Supporting Information). Interestingly, the peak in the spectrum of wild- type GFP
21 at 77 K is found at $(21230 \pm 100) \text{ cm}^{-1}$,⁷ resulting in a shift of the peak by the protein environment
22 by $+300 \text{ cm}^{-1}$ (see Figure 4). With increasing temperature, a prominent shoulder below the band
23 origin develops at 180 K into a partially resolved peak at $(20700 \pm 25) \text{ cm}^{-1}$ (483.1 nm), which
24 dominates the spectrum at 300 K. This low-energy features could be due to hot bands. However,
25 our Franck-Condon simulations do not recover the observed evolution of a second discernible low-
26 energy peak, regardless of the simulation temperature, consistent with Franck-Condon simulations
27 by others.^{22, 40-41} Alternatively, this low energy peak could be due to the presence of the *E* isomer.
28
29 Recent results by Bieske and coworkers observed the presence of the *E* isomer in ion mobility
30 experiments on HBDF⁻ ions prepared at room temperature³⁴ and presented evidence that the *E*
31 isomer absorbs at slightly longer wavelengths than the *Z* isomer. The barrier to interconversion
32 has been calculated to be 1.24 eV, which would hinder thermal isomerization.³⁴ Nonetheless, while
33 there remains some ambiguity regarding the origin of the low energy feature, we tentatively ascribe
34 it to the presence of the *E* isomer. Similar to the electronic band origin, the feature around 22000
35
36
37
38
39
40
41
42
43
44
45
46
47
48
49
50
51
52
53
54
55
56
57
58
59
60

1
2
3 cm^{-1} broadens and red-shifts with increasing temperature. We attribute this effect to the *E* isomer
4
5 having overall a similar Franck-Condon progression as the *Z* isomer (see Supporting Information).
6
7

8
9 Subtle differences between the envelope of the spectra of bare and N_2 -tagged HBDI^-
10 warrant some consideration. The relative intensities of the feature around 22000 cm^{-1} and of the
11 $\text{S}_1(v=0) \leftarrow \text{S}_0(v=0)$ band are different for $[\text{HBDI}^- \cdot \text{N}_2]$ compared to bare HBDI^- . This difference
12
13 could be due to a change in the Franck-Condon factors upon addition of an N_2 tag, although this
14
15 seems unlikely given the small perturbation that the N_2 tag induces. Alternatively, it could be
16
17 caused by a change in the branching ratio of internal conversion versus electron detachment. The
18
19 adiabatic electron affinity of HBDI^- is 22017 cm^{-1} .³⁷ Moreover, vibrational autodetachment from
20
21 the S_1 state has been observed to be a significant decay channel in HBDI^- (at 300 K) excited at
22
23 19600 cm^{-1} and higher.^{10, 18-21, 24, 26-28, 31} However, a direct comparison of parent ion depletion and
24
25 fragment action for bare HBDI^- shows that electron detachment does not significantly contribute
26
27 to the photodestruction of the ion at 30 K trap temperature (see Supporting Information). The
28
29 overall band contour of the spectrum of cryogenically prepared HBDI^- also compares very well
30
31 with the absorption spectrum of wild-type GFP at 77 K (see Figure 4),^{7, 44} for which
32
33 photodetachment is not possible in the visible, suggesting that photodetachment plays only a minor
34
35 role at low temperatures in the spectral range probed here. We suggest that the change in the
36
37 envelope of the spectrum could be caused by differences in *ion* temperature between $[\text{HBDI}^- \cdot \text{N}_2]$
38
39 and bare HBDI^- despite similar *trap* temperatures. The presence of the N_2 tag limits the internal
40
41 energy of the complex to a maximum of ca. 720 cm^{-1} , which is not the case for the bare ion, and
42
43 radiofrequency heating could introduce hot bands in the bare ion that are quenched by the presence
44
45 of an N_2 tag.
46
47
48
49
50
51
52
53
54
55
56
57
58
59
60

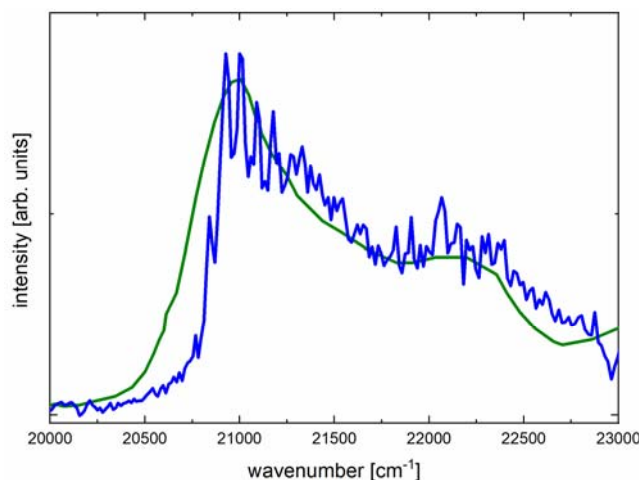


Figure 4. Comparison of the experimental spectrum of HBDF⁻ at 30 K trap temperature (blue line) with the absorption spectrum of wild-type GFP (green line). The absorption spectrum of wild-type GFP shown here represents the deconvoluted absorption spectrum attributed to the deprotonated state of the chromophore (digitized from Figure 2a in ref. ⁷). The wild-type GFP spectrum has been shifted by -300 cm^{-1} to optimally match the experimental spectrum of HBDF⁻.

Summarizing, we have removed many of the ambiguities in the photodissociation action spectrum of the chromophore of GFP by performing experiments on ions prepared in a cryogenic ion trap. The $S_1(v=0) \leftarrow S_0(v=0)$ transition of *Z*-HBDF⁻ is at $(20930 \pm 15)\text{ cm}^{-1}$ and the band shows partially resolved vibrational structure that are assigned to specific Franck-Condon active modes. At higher ion temperatures, it is likely that the *E* isomer of HBDF⁻ is observed, tentatively assigning its $S_1(v=0) \leftarrow S_0(v=0)$ transition to a feature that is red-shifted by $(230 \pm 30)\text{ cm}^{-1}$ compared to the *Z* isomer. At room temperature, this low energy feature is dominant in our experiment. These results highlight the importance of acquiring action spectra under well-controlled conditions and suggests that previous studies on HBDF⁻ may need to be revisited. Finally, the high-resolution spectrum measured here serves as a benchmark for theoretical studies that can now provide detailed insight into the S_1 state of *Z*-HBDF⁻ in the Franck-Condon region.

Experimental and Computational Methods

Solutions were prepared by dissolving HBDI in methanol with the pH adjusted to 11-12 by adding a few drops of aqueous KOH (ca. 50 mM), resulting in a dark yellow to orange solution. The solution was electrosprayed without further purification using N₂ as nebulizing gas. The spray enters a heated desolvation capillary at the entrance of a sequence of differential pumping stages where residual solvent molecules are evaporated resulting in bare ions. After leaving the heated capillary, the ions pass through a set of skimmers and a series of octopole ion guides before injection into a 3D quadrupole ion trap. This ion trap is mounted on a closed cycle helium cryostat and is equipped with a resistive heater to allow temperature control from room temperature down to 20 K. The ions are stored in this trap with D₂ buffer gas for 100 ms to cool them down to cryogenic temperatures. In the cryogenic ion trap, we form complexes of [HBDI⁺·(N₂)_n] (*n* = 0 - 2). The complexes are injected into a time-of-flight mass spectrometer where we mass select target ions using a pulsed mass gate. These mass selected ions are then irradiated with the output of a tunable optical parametric converter with pulse durations of 5-7 ns. The light source for spectroscopy in the visible spectral range is a BBO optical parametric oscillator with a bandwidth of ca. 5 cm⁻¹. For infrared spectroscopy we use a KTP/KTA/AgGaSe₂ based optical parametric converter system with a bandwidth of ca. 2 cm⁻¹. Fragmentation upon absorption of a photon is monitored using a reflectron for secondary mass analysis with a microchannel plate detector for fragment ion detection. Care was taken to ensure that the laser pulse energies used were sufficiently low to avoid significant multiphoton absorption.

1
2
3 The mass spectrometer was operated at a repetition rate of 10 Hz and the light source was
4 fired every other cycle to allow subtraction of background from unimolecular decay by monitoring
5 of fragment ion signal with and without the laser. All spectra were corrected for photon fluence,
6 where the spectra of [HBDI⁻·N₂] were corrected assuming a one-photon process, while spectra of
7 bare HBDI⁻ were corrected assuming that the dissociation is a two-photon process.
8
9
10
11
12
13
14

15 Geometry optimizations and harmonic frequency calculations for the ground state were
16 carried out using density functional theory (DFT) with the B3LYP functional⁴⁵ with a def2-TZVPP
17 basis set⁴⁶ for all atoms. As previously noted by others, there is a strong basis set dependence of
18 the IR features,³⁹ but we found in exploratory calculations that this problem only occurs for smaller
19 basis sets than the one used here. Excited states were calculated using the range-corrected CAM-
20 B3LYP functional.⁴⁷ Franck-Condon simulations were performed using results from the excited
21 state calculations. The simulation temperature is 55 K, the full width at half-maximum (FWHM)
22 of the vibrational features is 80 cm⁻¹, and the frequency ω_B was set to 65 cm⁻¹ on the S₁ surface to
23 fit the observed vibrational structure. Vertical excitation calculations using both CAM-B3LYP and
24 ω -B97X-D⁴⁸ functionals yield similar results that overestimate the electronic band origin by about
25 0.5 eV for the Z isomer. We shifted the calculated vertical excitation energies by ca. -4000 cm⁻¹ to
26 match the calculated vibronic progression with the experimental spectrum of [HBDI⁻·N₂]. All
27 calculations were carried out in Gaussian 16.⁴⁹
28
29
30
31
32
33
34
35
36
37
38
39
40
41
42
43
44
45
46
47
48
49

50 ASSOCIATED CONTENT

51
52
53 **Supporting Information.** Vibrational mode assignments for [HBDI⁻·N₂]; comparison of the
54 experimental spectrum of [HBDI⁻·N₂] with calculated spectra from the literature;
55
56
57
58
59
60

1
2
3 photodissociation action spectrum of [HBDI·(N₂)]; Franck-Condon simulation of the S₁ ← S₀
4 transition of the *E* isomer of HBDI; comparison of action and depletion spectra for HBDI;
5
6 optimized geometry of the ground state of the *Z* isomer; optimized geometry of the S₁ state of the
7
8 *Z* isomer; optimized geometry of the ground state of the *E* isomer; optimized geometry of the S₁
9
10 state of the *E* isomer; calculated vibrational frequencies (unscaled) in cm⁻¹.
11
12
13
14
15
16
17
18

19 AUTHOR INFORMATION

20 Corresponding Author

21
22 *E-mail: weberjm@jila.colorado.edu. Tel.: +1-303-492-7841
23
24
25
26
27

28 The authors declare no competing financial interests.
29
30
31
32

33 ACKNOWLEDGMENTS

34
35 We gratefully acknowledge support from the U. S. National Science Foundation under award no.
36
37 CHE-1764191, the NSF Physics Frontier Center at JILA (award no. PHY-1734006), and JILA for
38
39 a Visiting Fellowship to J.R.R.V. We also thank Drs. Stephen R. Meech and Philip C. B. Page
40
41 (University of East Anglia, UK, grant support through EPSCR grants EP/E010466 and
42
43 EP/H025715) for providing us with the *p*-hydroxybenzylidene-2,3-dimethylimidazolinone
44
45 samples that were used in this work.
46
47
48
49
50
51
52
53
54
55
56
57
58
59
60

REFERENCES

1. Chalfie, M.; Tu, Y.; Euskirchen, G.; Ward, W. W.; Prasher, D. C. Green fluorescent protein as a marker for gene-expression. *Science* **1994**, *263*, 802-805.
2. Tsien, R. Y. The green fluorescent protein. *Annu. Rev. Biochem.* **1998**, *67*, 509-544.
3. Hein, B.; Willig, K. I.; Hell, S. W. Stimulated emission depletion (STED) nanoscopy of a fluorescent protein-labeled organelle inside a living cell. *Proc. Natl. Acad. Sci. USA* **2008**, *105*, 14271-14276.
4. Day, R. N.; Davidson, M. W. The fluorescent protein palette: tools for cellular imaging. *Chem. Soc. Rev.* **2009**, *38*, 2887-2921.
5. Chudakov, D. M.; Matz, M. V.; Lukyanov, S.; Lukyanov, K. A. Fluorescent proteins and their applications in imaging living cells and tissues. *Physiol. Rev.* **2010**, *90*, 1103-1163.
6. Heim, R.; Prasher, D. C.; Tsien, R. Y. Wavelength mutations and posttranslational autooxidation of green fluorescent protein. *Proc. Natl. Acad. Sci. USA* **1994**, *91*, 12501-12504.
7. Chattoraj, M.; King, B. A.; Bublitz, G. U.; Boxer, S. G. Ultra-fast excited state dynamics in green fluorescent protein: Multiple states and proton transfer. *Proc. Natl. Acad. Sci. USA* **1996**, *93*, 8362-8367.
8. Mandal, D.; Tahara, T.; Meech, S. R. Excited-state dynamics in the green fluorescent protein chromophore. *J. Phys. Chem. B* **2004**, *108*, 1102-1108.

1
2
3 9. Litvinenko, K. L.; Webber, N. M.; Meech, S. R. Internal conversion in the chromophore
4 of the green fluorescent protein: Temperature dependence and isoviscosity analysis. *J. Phys.*
5
6 *Chem. A* **2003**, *107*, 2616-2623.

7
8
9
10 10. Forbes, M. W.; Jockusch, R. A. Deactivation pathways of an isolated green fluorescent
11 protein model chromophore studied by electronic action spectroscopy. *J. Am. Chem. Soc.* **2009**,
12
13 *131*, 17038-17039.

14
15 11. Voliani, V.; Bizzarri, R.; Nifosi, R.; Abbruzzetti, S.; Grandi, E.; Viappiani, C.; Beltram, F.
16 Cis-trans photoisomerization of fluorescent-protein chromophores. *J. Phys. Chem. B* **2008**, *112*,
17
18 10714-10722.

19
20 12. Kaucikas, M.; Tros, M.; van Thor, J. J. Photoisomerization and proton transfer in the
21 forward and reverse photoswitching of the fast-switching M159T mutant of the Dronpa fluorescent
22 protein. *J. Phys. Chem. B* **2015**, *119*, 2350-2362.

23
24 13. Nielsen, S. B.; Lapierre, A.; Andersen, J. U.; Pedersen, U. V.; Tomita, S.; Andersen, L. H.
25 Absorption spectrum of the green fluorescent protein chromophore anion in vacuo. *Phys. Rev. Lett.*
26
27 **2001**, *87*.

28
29 14. Andersen, L. H.; Lapierre, A.; Nielsen, S. B.; Nielsen, I. B.; Pedersen, S. U.; Pedersen, U.
30 V.; Tomita, S. Chromophores of the green fluorescent protein studied in the gas phase. *Eur. Phys.*
31
32 *J. D* **2002**, *20*, 597-600.

33
34 15. Andersen, L. H.; Bluhme, H.; Boye, S.; Jorgensen, T. J. D.; Krogh, H.; Nielsen, I. B.;
35 Nielsen, S. B.; Svendsen, A. Experimental studies of the photophysics of gas-phase fluorescent
36 protein chromophores. *Phys. Chem. Chem. Phys.* **2004**, *6*, 2617-2627.

1
2
3 16. Lammich, L.; Petersen, M. A.; Nielsen, M. B.; Andersen, L. H. The gas-phase absorption
4 spectrum of a neutral GFP model chromophore. *Biophys. J.* **2007**, *92*, 201-207.
5
6

7
8 17. Chingin, K.; Balabin, R. M.; Frankevich, V.; Barylyuk, K.; Nieckarz, R.; Sagulenko, P.;
9 Zenobi, R. Absorption of the green fluorescent protein chromophore anion in the gas phase studied
10 by a combination of FTICR mass spectrometry with laser-induced photodissociation spectroscopy.
11
12
13
14
15
16
17
18
19
20
21
22
23
24
25
26
27
28
29
30
31
32
33
34
35
36
37
38
39
40
41
42
43
44
45
46
47
48
49
50
51
52
53
54
55
56
57
58
59
60

Int. J. Mass Spectrom. **2011**, *306*, 241-245.

18 18. Forbes, M. W.; Nagy, A. M.; Jockusch, R. A. Photofragmentation of and electron
19 photodetachment from a GFP model chromophore in a quadrupole ion trap. *I. J. Mass Spectrom.*
20
21
22
23
24
25
26
27
28
29
30
31
32
33
34
35
36
37
38
39
40
41
42
43
44
45
46
47
48
49
50
51
52
53
54
55
56
57
58
59
60

2011, *308*, 155-166.

26 19. Horke, D. A.; Verlet, J. R. R. Photoelectron spectroscopy of the model GFP chromophore
27 anion. *Phys. Chem. Chem. Phys.* **2012**, *14*, 8511-8515.
28
29
30
31
32
33
34
35
36
37
38
39
40
41
42
43
44
45
46
47
48
49
50
51
52
53
54
55
56
57
58
59
60

32 20. Mooney, C. R. S.; Sanz, M. E.; McKay, A. R.; Fitzmaurice, R. J.; Aliev, A. E.; Caddick,
33 S.; Fielding, H. H. Photodetachment spectra of deprotonated fluorescent protein chromophore
34 anions. *J. Phys. Chem. A* **2012**, *116*, 7943-7949.
35
36
37
38
39
40
41
42
43
44
45
46
47
48
49
50
51
52
53
54
55
56
57
58
59
60

40 21. Toker, Y.; Rahbek, D. B.; Klaerke, B.; Bochenkova, A. V.; Andersen, L. H. Direct and
41 indirect electron emission from the green fluorescent protein chromophore. *Phys. Rev. Lett.* **2012**,
42
43
44
45
46
47
48
49
50
51
52
53
54
55
56
57
58
59
60

109.

47 22. Bochenkova, A. V.; Andersen, L. H. Ultrafast dual photoresponse of isolated biological
48 chromophores: link to the photoinduced mode-specific non-adiabatic dynamics in proteins.
49
50
51
52
53
54
55
56
57
58
59
60

Faraday Disc. **2013**, *163*, 297-319.

1
2
3 23. Mooney, C. R. S.; Horke, D. A.; Chatterley, A. S.; Simperler, A.; Fielding, H. H.; Verlet,
4 J. R. R. Taking the green fluorescence out of the protein: dynamics of the isolated GFP
5 chromophore anion. *Chem. Sci.* **2013**, *4*, 921-927.
6
7

8
9
10 24. West, C. W.; Hudson, A. S.; Cobb, S. L.; Verlet, J. R. R. Communication: Autodetachment
11 versus internal conversion from the S₁ state of the isolated GFP chromophore anion. *J. Chem.*
12 *Phys.* **2013**, *139*, 071104.
13
14
15

16
17
18 25. Bochenkova, A. V.; Klaerke, B.; Rahbek, D. B.; Rajput, J.; Toker, Y.; Andersen, L. H. UV
19 excited-state photoresponse of biochromophore negative ions. *Angew. Chem. Int. Ed.* **2014**, *53*,
20 9797-9801.
21
22
23

24
25
26 26. Mooney, C. R. S.; Parkes, M. A.; Zhang, L. J.; Hailes, H. C.; Simperler, A.; Bearpark, M.
27 J.; Fielding, H. H. Competition between photodetachment and autodetachment of the 2 ¹ππ* state
28 of the green fluorescent protein chromophore anion. *J. Chem. Phys.* **2014**, *140*, 205103.
29
30
31

32
33
34 27. West, C. W.; Bull, J. N.; Hudson, A. S.; Cobb, S. L.; Verlet, J. R. R. Excited State
35 Dynamics of the isolated green fluorescent protein chromophore anion following UV excitation.
36 *J. Phys. Chem. B* **2015**, *119*, 3982-3987.
37
38
39

40
41
42 28. Anstöter, C. S.; Bull, J. N.; Verlet, J. R. R. Ultrafast dynamics of temporary anions probed
43 through the prism of photodetachment. *Int. Rev. Phys. Chem.* **2016**, *35*, 509-538.
44
45
46

47
48 29. Kiefer, H. V.; Pedersen, H. B.; Bochenkova, A. V.; Andersen, L. H. Decoupling electronic
49 versus nuclear photoresponse of isolated green fluorescent protein chromophores using short laser
50 pulses. *Phys. Rev. Lett.* **2016**, *117*, 243004.
51
52
53

1
2
3 30. Anstöter, C. S.; Dean, C. R.; Verlet, J. R. R. Chromophores of chromophores: a bottom-up
4 Hückel picture of the excited states of photoactive proteins. *Phys. Chem. Chem. Phys.* **2017**, *19*,
5
6 29772-29779.
7
8

9
10
11 31. Bochenkova, A. V.; Mooney, C. R. S.; Parkes, M. A.; Woodhouse, J. L.; Zhang, L. J.;
12 Lewin, R.; Ward, J. M.; Hailes, H. C.; Andersen, L. H.; Fielding, H. H. Mechanism of resonant
13 electron emission from the deprotonated GFP chromophore and its biomimetics. *Chem. Sci.* **2017**,
14
15 8, 3154-3163.
16
17
18

19
20
21 32. McLaughlin, C.; Assmann, M.; Parkes, M. A.; Woodhouse, J. L.; Lewin, R.; Hailes, H. C.;
22 Worth, G. A.; Fielding, H. H. ortho and para chromophores of green fluorescent protein:
23 controlling electron emission and internal conversion. *Chem. Sci.* **2017**, *8*, 1621-1630.
24
25
26
27

28
29 33. Tay, J.; Parkes, M. A.; Addison, K.; Chan, Y. H.; Zhang, L. J.; Hailes, H. C.; Page, P. C.
30 B.; Meech, S. R.; Blancafort, L.; Fielding, H. H. The Effect of conjugation on the competition
31 between internal conversion and electron detachment: a comparison between green fluorescent
32 and red Kaede protein chromophores. *J. Phys. Chem. Lett.* **2017**, *8*, 765-771.
33
34
35
36
37

38
39 34. Carrascosa, E.; Bull, J. N.; Scholz, M. S.; Coughlan, N. J. A.; Olsen, S.; Wille, U.; Bieske,
40 E. J. Reversible photoisomerization of the isolated green fluorescent protein chromophore. *J. Phys.*
41
42 *Chem. Lett.* **2018**, *9*, 2647-2651.
43
44
45

46
47 35. Langeland, J.; Kjaer, C.; Andersen, L. H.; Nielsen, S. B. The effect of an electric field on
48 the spectroscopic properties of the isolated green fluorescent protein chromophore anion.
49
50 *ChemPhysChem* **2018**, *19*, 1686-1690.
51
52
53
54
55
56
57
58
59
60

- 1
2
3 36. Henley, A.; Fielding, H. H. Anion photoelectron spectroscopy of protein chromophores.
4
5 *Int. Rev. Phys. Chem.* **2019**, *38*, 1-34.
6
7
8
9 37. Deng, S. H. M.; Kong, X. Y.; Zhang, G. X.; Yang, Y.; Zheng, W. J.; Sun, Z. R.; Zhang, D.
10 Q.; Wang, X. B. Vibrationally resolved photoelectron spectroscopy of the model GFP
11 chromophore anion revealing the photoexcited S₁ state being both vertically and adiabatically
12 bound against the photodetached D₀ continuum. *J. Phys. Chem. Lett.* **2014**, *5*, 2155-2159.
13
14
15
16
17
18 38. Klots, C. E. Temperatures of evaporating clusters. *Nature* **1987**, *327*, 222-223.
19
20
21
22 39. Almasian, M.; Grzetic, J.; Berden, G.; Bakker, B.; Buma, W. J.; Oomens, J. Gas-phase
23 infrared spectrum of the anionic GFP-chromophore. *Int. J. Mass Spectrom.* **2012**, *330*, 118-123.
24
25
26
27 40. Martin, M. E.; Negri, F.; Olivucci, M. Origin, nature, and fate of the fluorescent state of
28 the green fluorescent protein chromophore at the CASPT2//CASSCF resolution. *J. Am. Chem.*
29 *Soc.* **2004**, *126*, 5452-5464.
30
31
32
33
34
35 41. Kamarchik, E.; Krylov, A. I. Non-Condon effects in the one- and two-photon absorption
36 spectra of the green fluorescent protein. *J. Phys. Chem. Lett.* **2011**, *2*, 488-492.
37
38
39
40 42. Dodson, L. G.; Zagorec-Marks, W.; Xu, S.; Smith, J. E. T.; Weber, J. M. Intrinsic
41 photophysics of nitrophenolate ions studied by cryogenic ion spectroscopy. *Phys. Chem. Chem.*
42 *Phys.* **2018**, *20*, 28535-28543.
43
44
45
46
47
48 43. Xu, S.; Smith, J. E. T.; Weber, J. M. The electronic spectrum of cryogenic ruthenium-tris-
49 bipyridine dications in vacuo. *J. Chem. Phys.* **2016**, *145*, 024304.
50
51
52
53 44. Bublitz, G.; King, B. A.; Boxer, S. G. Electronic structure of the chromophore in green
54 fluorescent protein (GFP). *J. Am. Chem. Soc.* **1998**, *120*, 9370-9371.
55
56
57
58
59
60

1
2
3 45. Becke, A. D. Density-Functional Exchange-energy approximation with correct
4 asymptotic-behavior. *Phys. Rev. A* **1988**, *38*, 3098-3100.

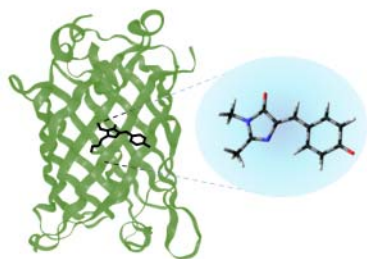
7
8
9 46. Weigend, F.; Ahlrichs, R. Balanced basis sets of split valence, triple zeta valence and
10 quadruple zeta valence quality for H to Rn: Design and assessment of accuracy. *Phys. Chem.*
11 *Chem. Phys.* **2005**, *7*, 3297-3305.

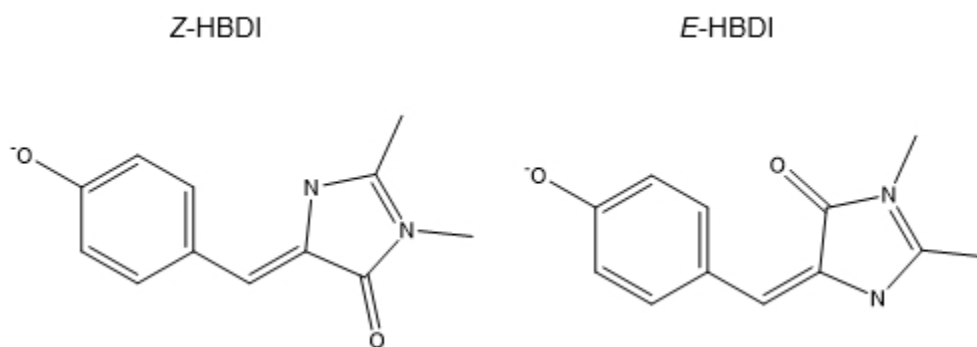
15
16 47. Yanai, T.; Tew, D. P.; Handy, N. C. A new hybrid exchange-correlation functional using
17 the Coulomb-attenuating method (CAM-B3LYP). *Chem. Phys. Lett.* **2004**, *393*, 51-57.

20
21 48. Chai, J.-D.; Head-Gordon, M. Long-range corrected hybrid density functionals with
22 damped atom–atom dispersion corrections. *Phys. Chem. Chem. Phys.* **2008**, *10*, 6615-6620.

26
27 49. Frisch, M. J.; Trucks, G. W.; Schlegel, H. B.; Scuseria, G. E.; Robb, M. A.; Cheeseman, J.
28 R.; Scalmani, G.; Barone, V.; Petersson, G. A.; Nakatsuji, H.; Li, X.; Caricato, M.; Marenich, A.
29 V.; Bloino, J.; Janesko, B. G.; Gomperts, R.; Mennucci, B.; Hratchian, H. P.; Ortiz, J. V.;
30 Izmaylov, A. F.; Sonnenberg, J. L.; Williams; Ding, F.; Lipparini, F.; Egidi, F.; Goings, J.; Peng,
31 B.; Petrone, A.; Henderson, T.; Ranasinghe, D.; Zakrzewski, V. G.; Gao, J.; Rega, N.; Zheng, G.;
32 Liang, W.; Hada, M.; Ehara, M.; Toyota, K.; Fukuda, R.; Hasegawa, J.; Ishida, M.; Nakajima, T.;
33 Honda, Y.; Kitao, O.; Nakai, H.; Vreven, T.; Throssell, K.; Montgomery Jr., J. A.; Peralta, J. E.;
34 Ogliaro, F.; Bearpark, M. J.; Heyd, J. J.; Brothers, E. N.; Kudin, K. N.; Staroverov, V. N.; Keith,
35 T. A.; Kobayashi, R.; Normand, J.; Raghavachari, K.; Rendell, A. P.; Burant, J. C.; Iyengar, S. S.;
36 Tomasi, J.; Cossi, M.; Millam, J. M.; Klene, M.; Adamo, C.; Cammi, R.; Ochterski, J. W.; Martin,
37 R. L.; Morokuma, K.; Farkas, O.; Foresman, J. B.; Fox, D. J. *Gaussian 16 Rev. C.01*, Wallingford,
38 CT, 2016.

1
2
3 **Table of Contents Graphic**
4
5
6
7





20 **Scheme 1.** *Z* and *E* isomers of HBDI.

21 84x33mm (150 x 150 DPI)

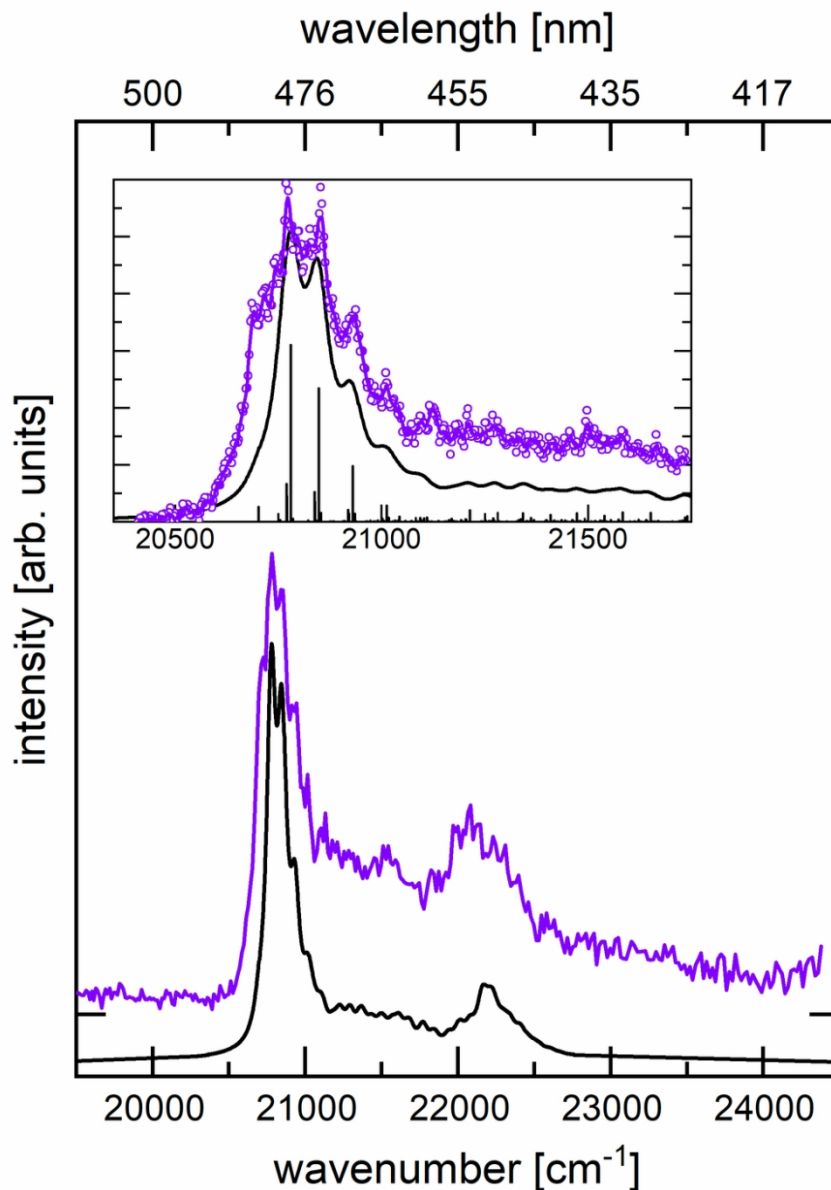


Figure 1. Photodissociation spectrum of [HBDI·N₂]. The open circles are raw data points, the purple full line is a 5-point adjacent average to guide the eye. The black full lines are Franck-Condon-Herzberg-Teller simulations of the vibrational substructure in the S₁ ← S₀ electronic band, with the vibrational states indicated as vertical sticks. The insert focuses on the band origin region, and the data in this trace were taken with a step size of 2.6 cm⁻¹, while the step size in the overview spectrum was 13 cm⁻¹. The simulation has been shifted by ca. -4000 cm⁻¹ for the best match to the experimental spectrum (see Methods section).

84x119mm (300 x 300 DPI)

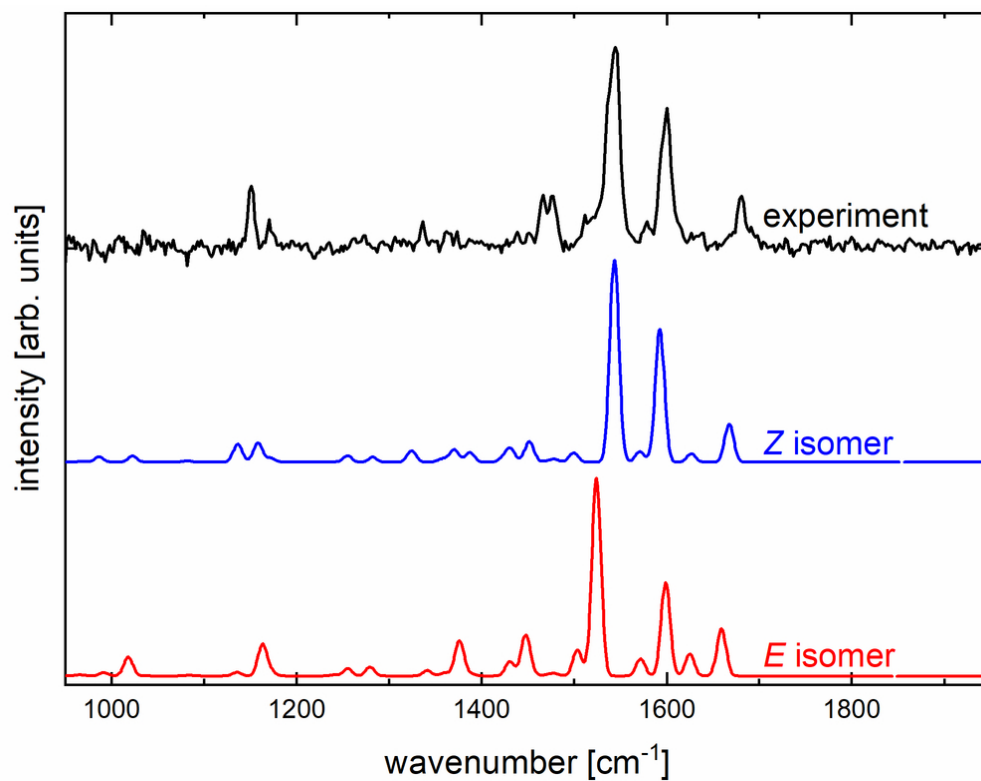


Figure 2. Experimental infrared action spectrum of $[\text{HBDI}^{\cdot-}\cdot\text{N}_2]$ (top trace) compared to simulated spectra of the *Z* isomer (center trace) and *E* isomer (bottom trace) of $\text{HBDI}^{\cdot-}$. The scaling factor for the simulated spectra is 0.98. A detailed assignment of the vibrational features is listed in Table S1 (see Supporting Information).

84x66mm (300 x 300 DPI)

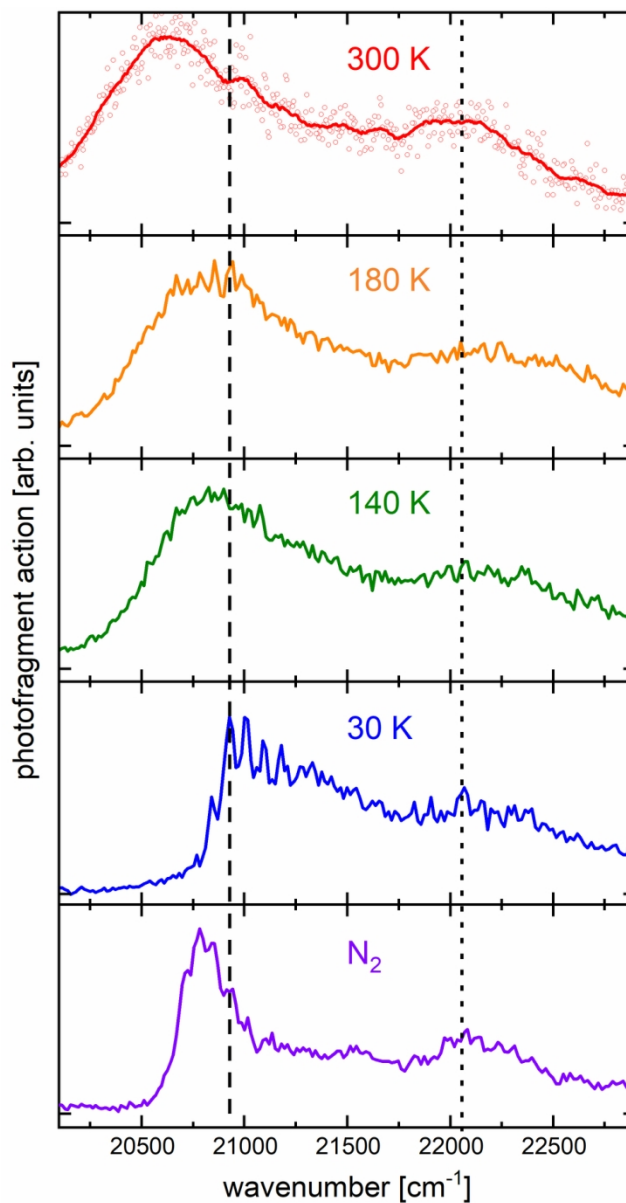


Figure 3. Photodissociation spectra of HBDI⁻ at different trap temperatures. For the spectrum at 300 K, the open circles are raw data points and the full line is a 20-point adjacent average to guide the eye. For the other spectra, the solid line represents the raw data. The vertical dashed and dotted lines shows the peak positions for bare HBDI⁻ (30 K) of the ($v=0$) \leftarrow ($v=0$) band at (20930 ± 10) cm⁻¹, and of the high energy feature around 22100 cm⁻¹, respectively.

84x158mm (300 x 300 DPI)

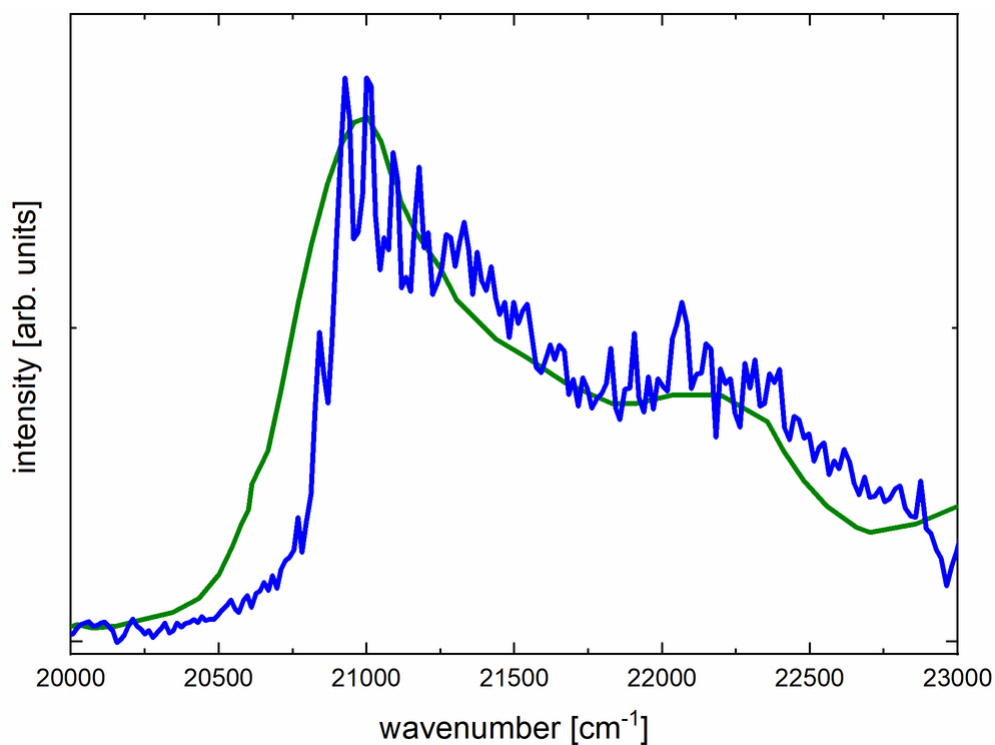
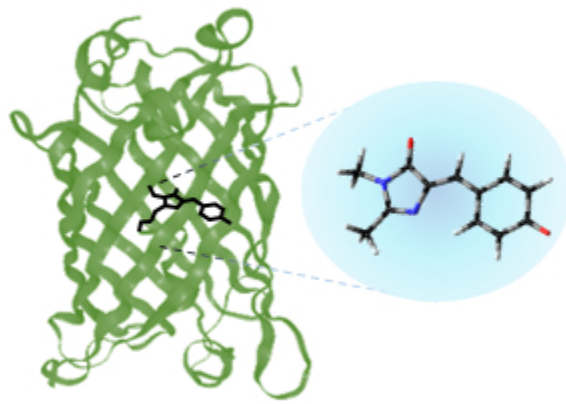


Figure 4. Comparison of the experimental spectrum of HBDI⁻ at 30 K trap temperature (blue line) with the absorption spectrum of wild-type GFP (green line). The absorption spectrum of wild-type GFP shown here represents the deconvoluted absorption spectrum attributed to the deprotonated state of the chromophore (digitized from Figure 2a in ref. 7). The wild-type GFP spectrum has been shifted by -300 cm^{-1} to optimally match the experimental spectrum of HBDI⁻.

84x62mm (300 x 300 DPI)

1
2
3
4
5
6
7
8
9
10
11
12
13
14
15
16
17
18
19
20
21
22
23
24
25
26
27
28
29
30
31
32
33
34
35
36
37
38
39
40
41
42
43
44
45
46
47
48
49
50
51
52
53
54
55
56
57
58
59
60



TOC Graphic

50x49mm (150 x 150 DPI)